Acta Geodaetica et Geophysica (2020) 55:237–255
https://doi.org/10.1007/s40328-020-00291-8

ORIGINAL STUDY

Research on the UWB/IMU fusion positioning of mobile vehicle based on motion constraints

Xin Li[1,2] · **Yang Wang**[1]

Received: 21 October 2019 / Accepted: 27 February 2020 / Published online: 3 March 2020

Abstract
In a non-line-of-sight (NLOS) environment, high accuracy ultra-wideband (UWB) positioning has been one of the hot topics in studying indoor positioning. Aiming at the UWB and inertial measurement unit (IMU) fusion vehicle positioning, a constraint robust iterate extended Kalman filter (CRIEKF) algorithm has been proposed in this paper. It has overcome the innate defect of the extended Kalman filter against non-Gaussian noise and the shortcoming of the robust extended Kalman filter algorithm, which has just processed the non-Gaussian noise solely based on the prior information. Our algorithm can update the observation covariance based on the posteriori estimate of the system in each iteration, and then update the posteriori distribution of the system based on the obtained covariance to significantly reduce the influence of non-Gaussian noise on positioning accuracy. Also, with the introduction of motion constraints, such as zero velocity, pseudo velocity and plane constraints, it can achieve a smoother positioning result. The experimental result proves that through the CRIEKF-based UWB/IMU fusion robot positioning method, a mean positioning accuracy of around 0.21 m can be achieved in NLOS environments.

Keywords UWB positioning · Motion constraint · Robust iterate Kalman filter · UWB/IMU fusing

1 Introduction

Currently, high positioning accuracy has been achieved through outdoor positioning technologies, especially the satellite-based navigation and positioning technology. However, there are still many problems in indoor navigation. Although great achievement has been made in WiFi, bluetooth, geomagnetism and UWB-based positioning technology, it's yet to be improved in positioning accuracy and reliability (Li et al. 2015, 2016; Santoso and Redmond 2015). The UWB-based indoor positioning can achieve a positioning accuracy of

✉ Xin Li
linuxcumt@126.com

[1] School of Computer Science and Technology, China University of Mining and Technology, Xuzhou 221116, People's Republic of China

[2] Mine Digitization Engineering Research Center of Ministry of Education, Xuzhou, People's Republic of China

around 0.3 m in LOS environments (García et al. 2015). However, the UWB base station is costly with large power, and prone to the influence of NLOS noise in a complex indoor environment, which would lead to a poor positioning accuracy (Zhang and Shen 2016).

The UWB/IMU fusion approach has been widely applied in some applications, where higher positioning accuracy is required. Sczyslo et al. (2008) and Fan et al. (2017) located pedestrians by fusing the UWB positioning result with IMU based on EKF. Xu and Chen (2016), Xu et al. (2016) and Fan et al. (2017) utilized the UWB measurements and the foot-mounted IMU or robot IMU for fusion positioning. Although the fusion result to some extent had improved the positioning accuracy, it was just a simple threshold method used to remove abnormal measurements. Wang et al. (2016) designed a tightly-coupled GPS/UWB/INS integrated positioning system based on the adaptive robust Kalman filter. However, their experiment was just carried out in outdoor LOS environments. Lukasz Zwirello et al. (2011) studied the EKF-based loosely/tightly coupled integration of UWB/INS based on the PDR algorithm. However, with this method, the positioning accuracy to a great extent was subject to the accuracy of the PDR algorithm itself. Benini et al. (2013) proposed a flying drone positioning approach by fusing vision, IMU and UWB. With the use of quick response (QR) codes in some specific indoor positions, the horizontal positioning accuracy could be as high as 10 cm.

With the continuous increase in the computing power of computing devices, particle filter (PF)-based fusion algorithms have been studied Wang et al. (2018) and Wang and Li (2017). Blanco et al. (2009) utilized PF to fuse the UWB, IMU and odometry data, and good positioning stability had been achieved in NLOS environments. Although PF can achieve high accuracy in a relatively less non-Gaussian noise environment (Nummiaro et al. 2003), the accuracy can also be greatly affected in the presence of strong interference, and the computational complexity is extremely high. In comparison, the EKF algorithm performs more efficiently in computation, which, however, is also prone to the interference from non-Gaussian noise. Although the Mahalanobis distance-based REKF was proposed to correct the UWB observation confidence for the suppression of non-Gaussian noise (Li et al. 2019), the UWB observation was just determined based on the prior information in the REKF algorithm. Under such a condition, if there's a big error in the system state, the reliability of the UWB observation will be affected.

In order to overcome the defect in REKF, RIEKF algorithm has been proposed for the IMU/UWB fusion robot positioning. The main innovation of this method lies in the correction of UWB observation confidence by integrating the prior information with all of the UWB observations through iterations. In the process of each iteration, the UWB observation confidence has been calculated based on the Mahalanobis distance. Owing to the repeated construction and solving of the marginal distribution, the final result will be a posteriori estimate based on all observations and prior distributions. Compared with REKF that relies solely on the prior information, this method can significantly improve the positioning accuracy and robustness. Finally, in order to further smooth the positioning result, a constraint method that includes pseudo velocity, zero velocity and plane constraint is presented.

The remainder of the paper is organized as follows: In Sect. 2, a UWB/IMU fusion algorithm is discussed, and the dynamic model, constraint observation model and UWB observation model for this algorithm are also presented. The pseudo velocity, zero velocity and plane constraints in the constraint observation model as well as the setting method of observation uncertainty in the UWB observation model based on RIEKF are mainly analyzed. Subsequently, several experiments are analyzed in Sect. 3, and Sect. 4 concludes the paper.

2 Analysis on IMU/UWB fusion positioning

2.1 Dynamic model

In a strapdown inertial navigation system (SINS), generally the IMU position, velocity and angle are estimated based on the EKF algorithm (Hol et al. 2009; Savioli et al. 2013; Ascher et al. 2011). The system state in the EKF at t moment is usually defined as:

$$X_t = \left[p_t, v_t, w_t, ba_t, bg_t\right]^T \tag{1}$$

where $\mathrm{p_t} = \left[\mathrm{x_t}, \mathrm{y_t}, \mathrm{z_t}\right]^{\mathrm{T}} \in \mathbb{R}^3$ is the three-axis coordinate of IMU, $\mathrm{v_t} = \left[\mathrm{v_{xt}}, \mathrm{v_{yt}}, \mathrm{v_{zt}}\right]^{\mathrm{T}} \in \mathbb{R}^3$ is the IMU velocity at the current moment, $\mathrm{w_t} = \left[\mathrm{w_{xt}}, \mathrm{w_{yt}}, \mathrm{w_{zt}}\right]^{\mathrm{T}} \in \mathbb{R}^3$ is the triaxial rotator at the current moment, $\mathrm{ba_t} = \left[\mathrm{ba_{xt}}, \mathrm{ba_{yt}}, \mathrm{ba_{zt}}\right]^{\mathrm{T}} \in \mathbb{R}^3$ is the acceleration deviation on three axes, and $\mathrm{bg_t} = \left[\mathrm{bg_{xt}}, \mathrm{bg_{yt}}, \mathrm{bg_{zt}}\right]^{\mathrm{T}} \in \mathbb{R}^3$ is the deviation of angular velocity on three axes. Actually, in order to avoid the problem of Gimbal lock in updating Euler angles, quaternion is usually adopted to express and calculate rotation (Fan et al. 2014). The quaternion at t moment is expressed as $q_t = \left[qw_t, qx_t, qy_t, qz_t\right]^T \in \mathbb{R}^4$, and the corresponding rotation matrix is indicated as $\mathcal{R}_t \in \mathbb{R}^{3\times3}$ for vector rotation. The uncertainty covariance matrix of the system state is denoted as $P_t \in \mathbb{R}^{15\times15}$.

The update of the IMU state is subject to the IMU sensor observation $u_t = \left[a_t^T g_t^T\right]^T \in \mathbb{R}^6$. $a_t = \left[a_{xt}, a_{yt}, a_{zt}\right]^T \in \mathbb{R}^3$ and $g_t = \left[g_{xt}, g_{yt}, g_{zt}\right]^T \in \mathbb{R}^3$ are separately the triaxial acceleration and the trialxial angular velocity at t moment. δT is used to indicate the length of time between $t-1 \rightarrow t$. The noise of the observation u_t conforms to the normal distribution when the covariance is Q_t and the mean value is 0 (Johnson and Sathyan 2011). The system state transition equation is defined as:

$$X_t = f\left(X_t, u_t\right) \tag{2}$$

It can be updated specifically according to the following formula:

$$q_t = \delta q \odot q_{t-1} \tag{3}$$

where $\odot$ is the quaternion multiply and δq is the quaternion update obtained based on the angular velocity. Then,

$$\delta q = \exp_q\left((g_t + bg_t) \times \delta T\right) \tag{4}$$

where $\exp_q()$ is the mapping from $\mathfrak{so}(3) \rightarrow \mathrm{SO}(3)$ in the relevant lie algebra. The approximate formula as below can be adopted during the calculation:

$$\delta q = \begin{bmatrix} \cos\frac{\left\|(g_t+bg_t)\times\delta T_2\right\|}{2} \\ \frac{\left((g_t+bg_t)\times\delta T\right)}{\left\|(g_t+bg_t)\times\delta T_2\right\|} \times \sin\frac{\left\|(g_t+bg_t)\times\delta T_2\right\|}{2} \end{bmatrix}^T \tag{5}$$

After the update, the rotation from the sensor coordinates to the navigation coordinate system can be obtained. Then, the acceleration can be transformed to the navigation coordinate system from the sensor coordinates for the update of the velocity and displacement.

$$v_t = v_t + la_t \times \delta T \tag{6}$$

$$p_t = p_{t-1} + \frac{1}{2} \times \left(v_t + v_{t-1}\right) \times \delta T \tag{7}$$

where la_t is the IMU acceleration in the navigation coordinate system, and its relationship with the gravitational acceleration and the IMU measurement meets the following formula:

$$la_t = \mathcal{R}_t\left(a_t + ba_t\right) + [00\mathcal{G}]^T \tag{8}$$

where, $\mathcal{G}$ is the local gravitational acceleration.

The covariance matrix of the system state can be updated according to the following formula:

$$P_t^- = F_t P_{t-1}^+ F_t^T + G_t Q_t G_t^T \tag{9}$$

And

$$F_t = \begin{bmatrix} I_3 & I_3 \times \delta T & 0_3 & 0_3 & 0_3 \\ 0_3 & I_3 & S_t \times \delta T & \mathcal{R}_t \times \delta T & 0_3 \\ 0_3 & 0_3 & I_3 & 0_3 & -\mathcal{R}_t \times \delta T \\ 0_3 & 0_3 & 0_3 & I_3 & 0_3 \\ 0_3 & 0_3 & 0_3 & 0_3 & I_3 \end{bmatrix} \tag{10}$$

$$G_t = \begin{bmatrix} 0_3 & 0_3 \\ \mathcal{R}_t \times \delta T & 0_3 \\ 0_3 & -\mathcal{R}_t \times \delta T \\ 0_3 & 0_3 \\ 0_3 & 0_3 \end{bmatrix} \tag{11}$$

where the diagonal line I_3 is the three-dimensional matrix of 1 and 0_3 is a three-dimensional matrix where all of the elements are 0. $S_t = \left[\left(\mathcal{R}_t a_t\right)^{\times}\right]$, where $()^{\times}$ means the following operation:

$$\left[w_1, w_2, w_3\right]^{\times} = \begin{bmatrix} 0 & -w_3 & w_2 \\ w_3 & 0 & -w_1 \\ -w_2 & w_1 & 0 \end{bmatrix} \tag{12}$$

2.2 Motion constraint model

Error can be accumulated continuously in a pure IMU positioning process, and it would lead to a large deviation in the positioning result. Especially, the growth of velocity error will significantly reduce the positioning accuracy. The main source of these problems is gravity 'leaking' into the acceleration input and corrupting the velocity vector (Titterton and Weston 2004). As soon as velocity drift occurs, position will gradually diverge. In this case, zero velocity, pseudo velocity and plane constraints can be introduced to control the cumulative error in an inertial navigation system.

(1) Zero velocity constraint

When IMU is used to position a four-wheeled robot and if the robot is temporarily motionless in the motion process, the velocity at this moment is approximately equal to 0. By this character, the growth of positioning error can be constrained. The zero-velocity state of a robot can be detected through the GLRT (Fischer et al. 2013). The main principle lies in calculating the variance between the acceleration measurement and the angular velocity measurement within the time window. It's considered as zero-velocity state when the variance is lower than a certain value. According to this, the velocity error in IMU integral won't monotonically increase over time.

The velocity in the zero-velocity state can be defined as $v_{zero} = [000]^T$ with the noise conforming to the Gaussian distribution and the covariance matrix is $O_{zero} \in \mathbb{R}^{3\times3}$.The system observation equation is linear:

$$y_{zeor} = H_{zero}X^T \tag{13}$$

$$H_{zero} = \begin{bmatrix} 0_{3\times3} & I_{3\times3} & 0_{3\times3} & 0_{3\times3} & 0_{3\times3} \end{bmatrix}^T \tag{14}$$

It can be updated according to the following formula:

$$K_{zero,t} = P_t^- H_{zeor}\left(O_{zero} + H_{zero}P_t^- H_{zero}^T\right)^{-1} \tag{15}$$

$$dX = K_{zero,t}\left(y_{zero} - v_{zero}\right) \tag{16}$$

$$X_t^- = Update\left(X_t^-, dX\right) \tag{17}$$

$$P_t^+ = \left(I - K_{zero,t}H_{zero}\right)P_t^- \tag{18}$$

where P_t^-, P_t^+ separately represent the prior covariance matrix and the posterior covariance matrix, X_t^-, X_t^+ are respectively the prior state and the posteriori state, and $dX = \left[dp_t dv_t dw_t dba_t dbg_t\right]^T \in \mathbb{R}^{15}$. *Updata*() is non-linear in a rotation operation with the specific formation provided as below:

$$\begin{cases} p_t^+ = p_t^- + dp_t \\ v_t^+ = v_t^- + dv_t \\ ba_t^+ = ba_t^- + dba_t \\ bg_t^+ = bg_t^- + dbg_t \\ q_t^+ = q_t^- \odot \exp_q\left(dw_t\right) \end{cases} \tag{19}$$

Here, the superscripts of all components have the same meaning with those as above, separately standing for the priori and the posteriori. With the zero-velocity constraint, the cumulative velocity error in filter can be effectively restrained. Also, the other system states, especially the accelerometer deviation and gyro deviation, namely ba_t and bg_t, can be corrected as well, which also improves the overall positioning accuracy.

(2) Pseudo-velocity constraint

In order to control velocity drift, a pseudo-velocity update formula is provided in this paper to prevent the system from accelerating to an unreasonably high value. Basically, velocity can be controlled in the range of several meters per second. The pseudo-velocity update model has been defined according to the Euclidean norm of velocity.

The pseudo-velocity update formula is defined as:

$$\begin{cases} v_{pseudo} = \left\| v_t \right\|_2, & t \le 20 \\ v_{pseudo} = \left\| v_{t-1} : v_{t-20} \right\|_2, & t > 20 \end{cases} \tag{20}$$

With noise conforming to the Gaussian distribution, the covariance matrix is $O_{pseudo} \in \mathbb{R}^{1\times 1}$.

The system observation equation is linear:

$$y_{pseudo} = H_{pseudo} X^T \tag{21}$$

$$H_{pseudo} = \left[0_{1\times 3} \;\; I_{1\times 3} / \left\| v_t \right\|_2 \;\; 0_{1\times 3} \;\; 0_{1\times 3} \;\; 0_{1\times 3} \right]^T \tag{22}$$

It can be updated as below:

$$K_{pseudo,t} = P_t^- H_{pseudo} \left(O_{zero} + H_{pseudo} P_t^- H_{pseudo}^T \right)^{-1} \tag{23}$$

$$dX = K_{pseudo,t} \left(y_{pseudo} - v_{pseudo} \right) \tag{24}$$

$$X_t^- = Update\left(X_t^-, dX \right) \tag{25}$$

$$P_t^+ = \left(I - K_{pseudo,t} H_{pseudo} \right) P_t^- \tag{26}$$

The pseudo-velocity and zero-velocity constraints cannot be applied simultaneously, which means that if zero-velocity constraint is applied at a specific moment t, the pseudo-velocity constraint won't be imposed then.

(3) Plane constraint

Plane constraint assumes that robot just moves on a plane to reduce the influence of the base station layout, which might lead to an inaccurate estimation of the z coordinates on the UWB observation.

The z coordinate under plane constraint is defined as $z_{plane} = p_0[3]$ and $\mathrm{p}_0[3]$ is the z coordinate of the UWB unit at the initial moment with the noise conforming to the Gaussian distribution. The covariance matrix is $\mathrm{O}_{\mathrm{plane}} \in \mathbb{R}$.

The system observation equation is linear:

$$y_{plane} = H_{plane} X^T \tag{27}$$

$$H_{plane} = \left[0_{1\times 5} \;\; 1 \;\; 0_{1\times 3} \;\; 0_{1\times 3} \;\; 0_{1\times 3} \right]^T \tag{28}$$

It can be updated according to the following formula:

$$K_{plane,t} = P_t^- H_{plane}\left(O_{zero} + H_{plane} P_t^- H_{plane}^T\right)^{-1} \tag{29}$$

$$dX = K_{plane,t}\left(y_{plane} - v_{plane}\right) \tag{30}$$

$$X_t^- = Update\left(X_t^-, dX\right) \tag{31}$$

$$P_t^+ = \left(I - K_{plane,t} H_{plane}\right) P_t^- \tag{32}$$

2.3 UWB update model

(1) Standard UWB observations

Assume that N UWB base stations have been used in the positioning process and the coordinate matrix of these base stations is expressed as $B_i \in \mathbb{R}^3$, where $B_i \in \mathbb{R}^3$ is the coordinate of the ith base station. If there are n UWB measurements observed at t moment, it will be defined as $m_t \in \mathbb{R}^n$, where $m_{t,i}$ is the ranging measurement of the ith base station at t moment, and $B_t \in \mathbb{R}^{n\times 3}$ is the coordinate of the measured base station at t moment.

Assume that the system state at t moment is X_t, whose coordinate is p_t and y_i is the observation of the ith base station, and then the system observation equation can be:

$$\mathrm{y_i} = \mathrm{h_i}\left(\mathrm{X_t}, \mathrm{n_t}\right) = \left\|\mathrm{p_t} - \mathrm{B_i}\right\|_2 + \mathrm{n_{t,i}} \tag{33}$$

$n_t \in \mathbb{R}^N$ is the observation noise and the observation noise of the ith base station is $n_{t,i} \sim N\left(0, R_{t,i}\right)$, where $R_{t,i}$ is the covariance matrix of the observations in the relevant base station at the current moment and $\|\|_2$ is the second-order model (L2-norm). Then, the Jacobian matrix of the state equation at X_t can be expressed as:

$$H_{X_t} = \left[H_{X_t,1}^T \ldots\ldots H_{X_t,n}^T\right]^T \tag{34}$$

where

$$H_{X_t,i} = \left[H_{p_t}^T\, Zero_3^T\, Zero_3^T\, Zero_3^T\, Zero_3^T\right]^T \tag{35}$$

is the Jacobian matrix of the observation equation in the ith base station, and $\mathrm{Zero_3} \in \mathbb{R}^3$ is a three-dimensional vector matrix, where all of the elements are 0.

$$H_{p_t} = \frac{\partial\left(h\left(p_t\right)\right)}{\partial\left(p_t\right)} = \frac{p_t - B_t}{\left\|p_t - B_t\right\|_2} \tag{36}$$

where p_t is a three-dimensional position coordinate in X_t.

(2) RIEKF-based UWB observations

The UWB observations in LOS environments conform to Gaussian noise. But in NLOS environments, the noise model can hardly be estimated due to the influence of various factors, such as refraction, the presence of barriers, etc. For this reason, REKF is introduced to eliminate the influence of noise signals. It uses Mahalanobis distance for the dynamic correction of observation or state covariance to reduce the influence of non-Gaussian noise on the positioning accuracy in NLOS environments.

Assume that it's a mean value when the UWB observation $m_{t,i}$ conforms to $h_i(X_t)$, and $H_{X_t,i}P_t^+H_{X_t,i}^T - R_{t,i}$ is the Gaussian distribution of the variance. Therefore, $\gamma_{t,i}$ the square of the Mahalanobis distance between $m_{t,i}$ and $h_i(X_t)$ conforms to the χ^2 distribution. So,

$$\gamma_{t,i} = \left(\mathrm{m_{t,i}} - h_i(X_t)\right)^T \left(H_{t,i}P_t^- H_{t,i}^T + R_{t,i}\right)^{-1} \left(m_{t,i} - h_i(X_t)\right) \sim \chi_1^2 \tag{37}$$

where χ_1^2 represents the conformity to the χ^2 distribution with a freedom degree of 1. It also means that the significance level α is given. Therefore,

$$\Pr\left(\gamma_{t,i} < \chi_{1,\alpha}^2\right) = 1 - \alpha \tag{38}$$

where Pr () is the probability of a random event, and $\chi_{1,\alpha}^2$ is the α-quantile of the χ^2 distribution with a freedom degree of 1. For those observations that fail to meet this condition, they'll be considered as outliers, whose influence on the posterior estimate can be reduced by an increase in the covariance. Compared with a standard Kalman filter, the difference lies in that this method can determine the observation covariance based on the prior state before the posterior state has been obtained.

Based on the iterated extended Kalman filter (IEKF), the local maximum posterior estimate on system state can be made through iterations to reduce the linear error in the observation equation. An RIEKF algorithm can be obtained if an update on the observation covariance should be added into the IEKF algorithm in each iteration. Compared with the REKF algorithm, which relies directly on the prior distribution to determine the observation covariance, the algorithm proposed in this paper can separately calculate the observation covariance and the posterior distribution of the system state through multiple iterations. It can utilize not only the prior distribution information but also all of the UWB observations in the same run.

The pseudo code of this new algorithm is shown in Algorithm 1. The current system state in each iteration is called the operate point, which is indicated by $\mathrm{X_{op}}$. The equation for iterative calculation at each operation point is shown as 4–11 in Algorithm 1. When the difference between $\mathrm{X_t^+}$ and $\mathrm{X_{op}}$ is small enough or the number of cycles exceeds a certain limit, it can be considered that the algorithm has converged.

Algorithm 1 Pseudo Code of Robust IEKF

1. Input P_t^-, X_t^-, m_t, B_t
2. Set $X_t^+ \coloneqq X_t^-$
3. Do
4. For each $m_{t,i}$:
5. Calculate $\gamma_{t,i}$ using Eq. (39)
6. Calculate $R'_{t,i}$ using Eq. (40)
7. Set $X_{op} \coloneqq X_t^+$
8. Set $P_t^- \coloneqq P_t^+$
9. $K = P_t^- H_{X_{op}} \left(H_{X_{op}} P_t^- H_{X_{op}}^T + R_t^{'} \right)^{-1}$
10. $P_t^+ = \left(I - K H_{X_{op}} \right) P_t^-$
11. $X_t^+ = X_t^- + K_t \left(m_t - h\left(X_{op}\right) - H_{X_{op}}\left(X_t^- - X_{op}\right) \right)$
12. While $\left\| X_t^+ - X_{op} \right\|_2 < \epsilon$
13. Return P_t^+, X_t^+

In order to reduce the influence of outliers and aiming at the current state of the operate point, the Mahalanobis distance between the observation and the system state can be calculated in each iteration to differentiate the outlier from the normal point, and update the observation covariance. As it's based on the system state of the current operate point and the posterior probability, $\gamma_{t,i}$ can be expressed as:

$$\gamma_{t,i} = \left(\mathrm{m_{t,i}} - h_i\left(X_{op}\right) \right)^T \left(H_{t,i} P_t^+ H_{t,i}^T + R_{t,i} \right)^{-1} \left(m_{t,i} - h_i\left(X_{op}\right) \right) \sim \chi_1^2 \tag{39}$$

Different from Formula (37) in the REKF algorithm, which calculates $\gamma_{t,i}$ based on the prior state and the observations, the RIEKF algorithm calculates $\gamma_{t,i}$ based on the various observations under the current covariance and the observation under the corresponding posterior distribution at the current operate point.

For large ranging observations, the covariance must be increased as well to reduce the influence on the posterior estimate. The new observation covariance matrix can be updated according to the following formula:

$$R'_{t,i} = \begin{cases} R_{t,i} & \gamma_{t,i} < \chi_{1,\alpha}^2 \\ \left(\frac{\gamma_{t,i}}{\chi_{1,\alpha}^2} \right) \times R_{t,i} & \gamma_{t,i} \geq \chi_{1,\alpha}^2 \end{cases} \tag{40}$$

where $\frac{\gamma_{t,i}}{\chi_{1,\alpha}^2}$ is the ratio between the Mahalanobis distance and the threshold when the observation is under the current covariance at the current operate point. It should be noted that the system state and the corresponding covariance matrix used in the first iteration are obtained based on the priori estimate in the RIEKF. But in the following iterations, the RIEKF algorithm updates the observation covariance based on the current system posterior estimate, which will then be updated according to the covariance obtained just now. To be specific, it means that according to 9–11 in Algorithm 1, the optimal linear solution is

obtained based on the given covariance. And, Formula (40) can be considered as an approximation calculation of the most suitable observation covariance under the given system state.

3 Experiments

In order to evaluate the accuracy of the positioning algorithms in NLOS environments, experiments were carried out in the entrance hall, School of Computer Science and Technology, China University of Mining and Technology, where totally four base stations had been established as indicated in Fig. 1. Decawave DWM1000 chip was used as the core chip of the UWB unit/base station, which was also fixed on the robot at a sampling frequency of 2 Hz. The x-IMU from X-IO Technologies, UK had been chosen as the IMU device, which was fixed at a position 5 cm below the UWB unit at a sampling frequency of 100 Hz. In order to maintain data synchronization between IMU and UWB, the notebook on the robot can simultaneously receive the ranging data from IMU and UWB, as indicated in Fig. 2.

In the experiment, the robot moved in an 8-shaped path and circled four times through the whole trajectory, as indicated in Fig. 3. Also, Fig. 3 shows the positions of four base stations indicated by rectangle points. As the real trajectory of the robot can hardly be obtained, the trajectory as below just serves as a reference diagram. Moreover, in order to increase the positioning noise in the 8-shaped path, the tester had randomly shielded 1–2 base stations, resulting in the anomaly or loss of ranging data in the base station.

It's denoted by UWB for the pure UWB positioning result, by EKF for the IMU/UWB fusion algorithm based on the standard EKF, by REKF for the fusion algorithm based on the Robust EKF, by RIEKF based on the Robust IEKF and by CRIEKF for the constraint robust IEKF-based fusion algorithm. In all of these positioning algorithms, both of the initial position and initial direction are pre-given. Due to the uncertainty of the real trajectory in the experiment, reference trajectory is used in this paper as the evaluation standard to compare the different algorithms in terms of the positioning accuracy. Also, in the

Fig. 1 The test field for UWB/IMU positioning

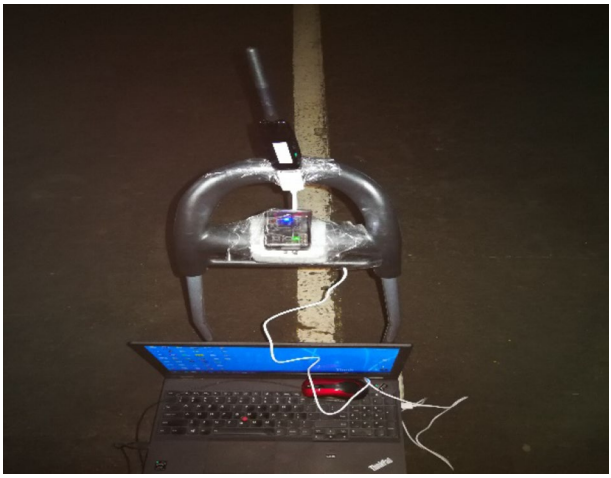

Fig. 2 The platform for the mobile robot

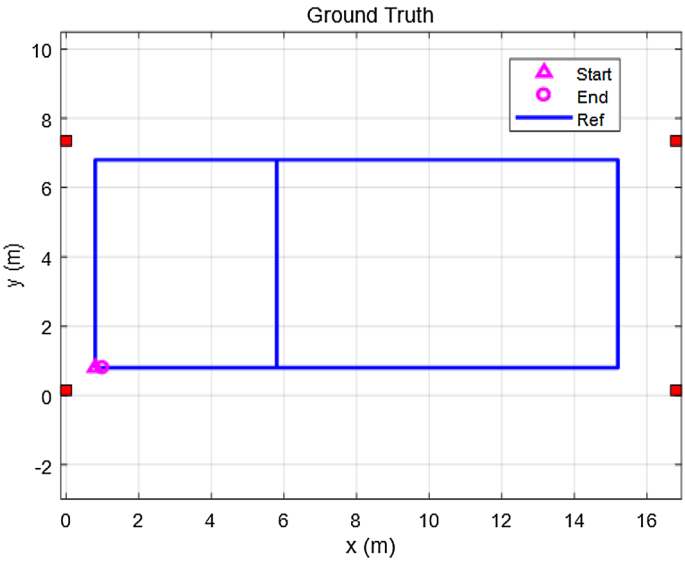

Fig. 3 Map of the experimental field and the reference trajectory

experiment, the same covariance parameter was used by all of the fusion algorithms in the same initial state.

3.1 NLOS analysis of raw data and positioning results of UWB

Throughout the whole process, the UWB data of four base stations are shown in Fig. 4, where the x-coordinate represents the time in seconds, while the y-coordinate represents the range in meters. If the range is less than 0.0 m, it means that the ranging data of the UWB base station in the current process are missing. It's very obvious that there are lots

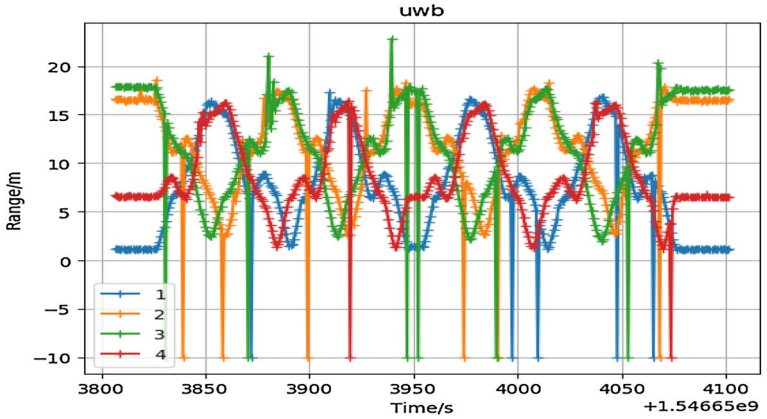

Fig. 4 UWB measurements

of NLOS noises, indicating the existence of abundant missing data and outliers, which, however, will affect the positioning result greatly.

The positioning result is shown in Fig. 5, where the above UWB data have been used to make the positioning. In all of the figures and trajectory diagrams as below, both of the x-coordinate and the y-coordinate will be measured in meters. The yellow and green lines separately represent the reference trajectory and the trajectory obtained based on the pure UWB positioning algorithm. It's very obvious that the UWB positioning trajectory has been affected by NLOS noise and big deviation has arisen. Therefore, high

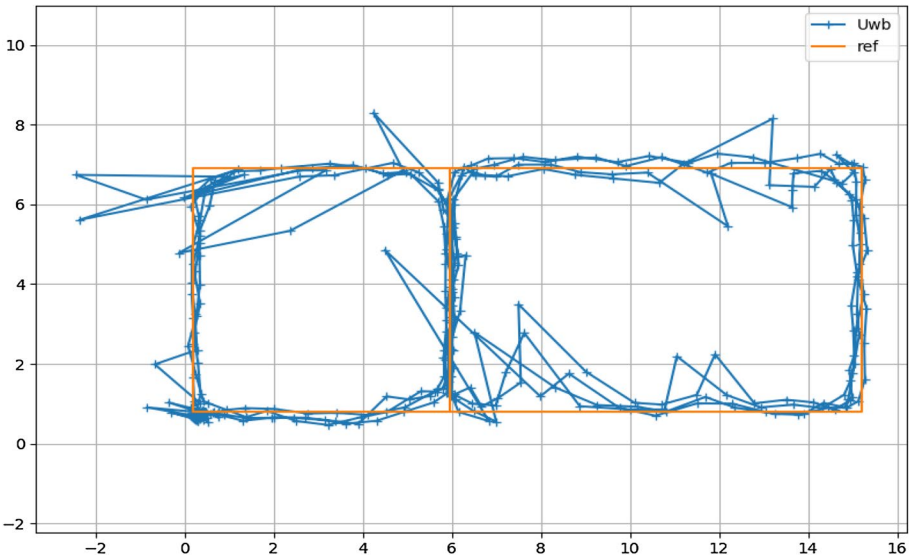

Fig. 5 The UWB positioning result

precision positioning can hardly be achieved based on the pure UWB data with a maximum error of up to about 3 m.

3.2 Analysis on the EKF-based positioning

As indicated in Fig. 6, the EKF algorithm has higher positioning accuracy than the UWB method after the fusion of IMU data because fixed observation covariance has been set with the standard EKF algorithm, which will also be used to estimate the maximum posterior distribution of the system state under this condition. The EKF algorithm can achieve good positioning accuracy in the area, where the UWB positioning method has performed quite well. However, in the NLOS region, the UWB measurement of the outliers will seriously affect the estimation on the posterior distribution. As indicated in the lower right part of Fig. 6, big deviation has arisen in the positioning trajectory.

3.3 Analysis on the REKF-based positioning

REKF algorithm can reduce the influence of outliers on its own by adjusting the observation covariance. However, if big error has occurred continuously on the UWB observations, it would lead to a large error on the system state to misjudge some correct ranging observations as error observations, which consequently would lead to an error in the observation covariance to reduce the positioning accuracy. As indicated in the lower right part of Fig. 7, due to the deviation of the system state, the system state failed to recover to normal in the next five meters. It was not until some normal UWB observations having been received successively that the system state was gradually corrected based on the correct observations. Actually, due to the deviation of system state now and then, some abnormal observations have been misjudged as correct observations. Also, due to the deviation of system state, the confidence of the correct observations might be very low. Therefore, it

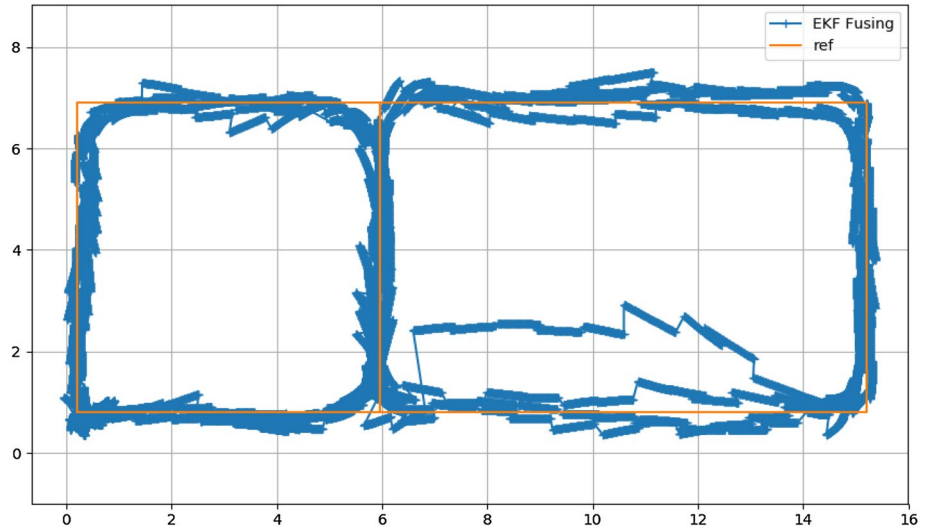

Fig. 6 The UWB/IMU fusion positioning result based on EKF

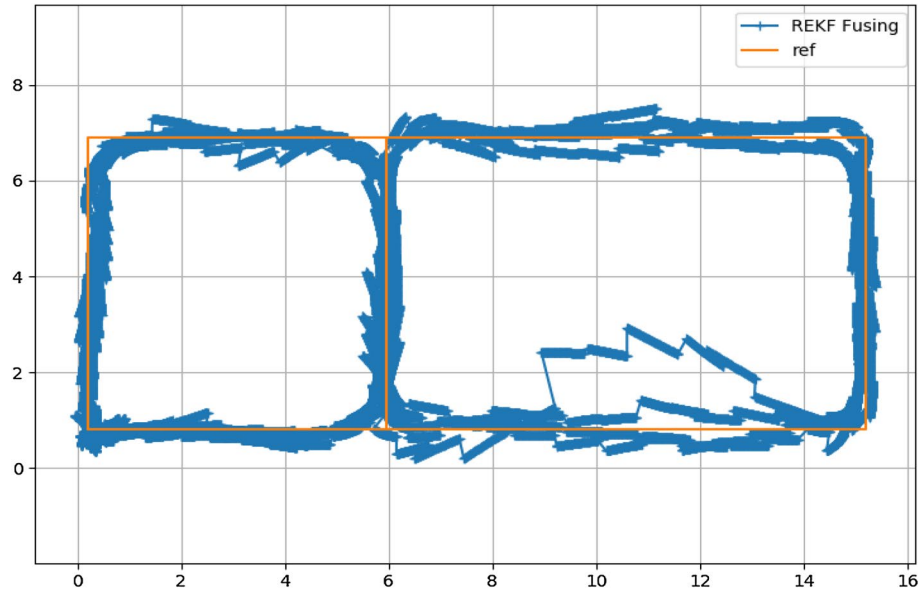

Fig. 7 The UWB/IMU fusion positioning result based on REKF

would be harder to recover to a correct state from an error state through the REKF algorithm than the EKF algorithm.

3.4 Analysis on RIEKF

As indicated in Fig. 8, the RIEKF algorithm can achieve an accurate positioning result. It updates the posterior distribution of the system and the observation covariance through repeated iterations. The posterior distribution obtained after each update contains all of the observation information and will be used to update the observation covariance. Therefore, in such a process of continuous iterations, not only the linear error can be eliminated, but also the correct estimation on the observation covariance can be made. In addition, with this character, the system state can be recovered to the normal state more quickly from the error estimate caused by abnormal observation because the observation covariance is determined based on the prior state and all of the observations. Therefore, when all of the observations are relatively more accurate, the posterior probability obtained thereof will be more approximate to the likelihood distribution, which will also speed up the correction of the error caused by false observation. This has been proved in the lower right part of Fig. 8. Therefore, although there are obvious outliers in this region, the RIEKF algorithm still can achieve a quick recovery in the following positioning process.

3.5 Analysis on CRIEKF

Firstly, the comparison between Figs. 9 and 10 shows that velocity changes more smoothly based on the pseudo-velocity and zero-velocity constraint with the peak velocity varying in the range around $\pm$ 1.25 m/s. But if there is no pseudo velocity constraint, the velocity

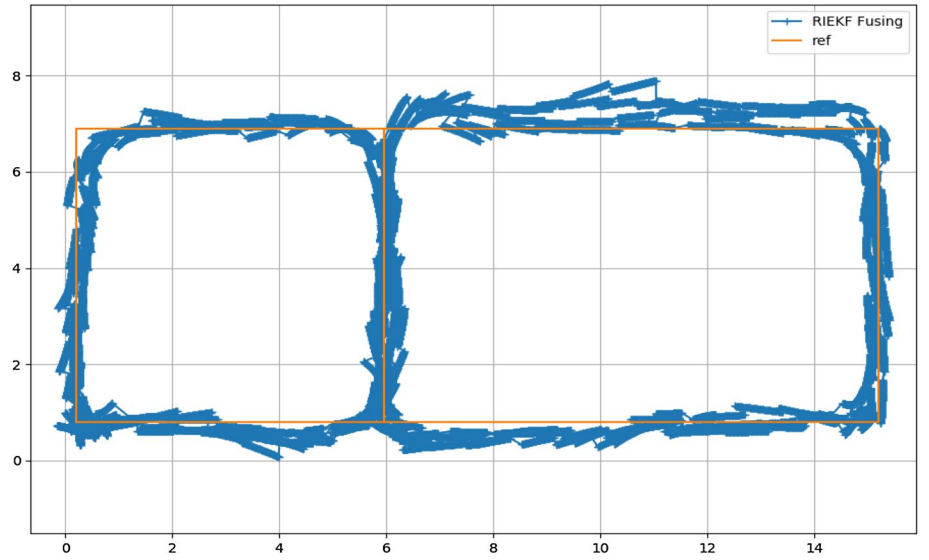

Fig. 8 The UWB/IMU fusion positioning result based on RIEKF

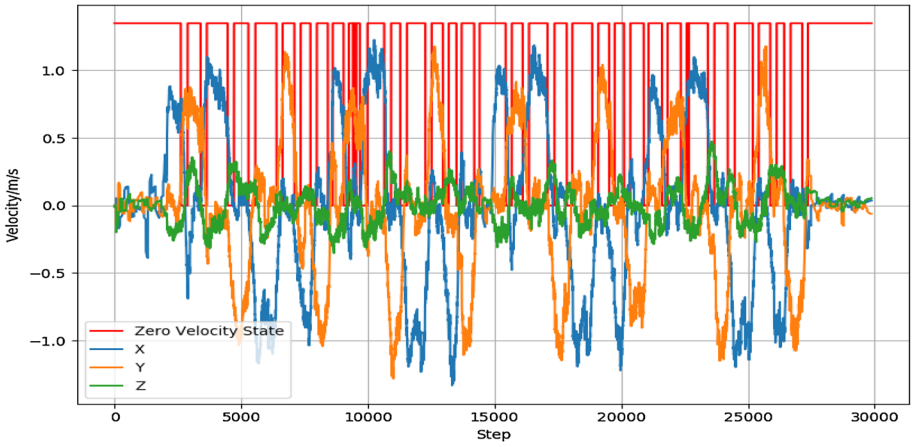

Fig. 9 The triaxial velocity based on the pseudo-velocity constraint

peak will change in the range around ± 1.5 m/s. Smooth velocity will bring about smoother trajectory. However, as indicated in Figs. 9 and 10 by the red line, as the robot was pulled by a person during the movement, it was in a transient zero-velocity state between the different steps.

As indicated in Fig. 11, the trajectory is smoother based on the velocity and plane constraints. In a local region, such as the area near the coordinate (1.0, 7.0), CRIEKF performs more stably than RIEKF. Now please pay attention to the velocity constraint. Covariance must be properly increased when the velocity is thought to be equal to the mean velocity in the previous time frame. In our experiment, the velocity covariance was set to be 6 m/

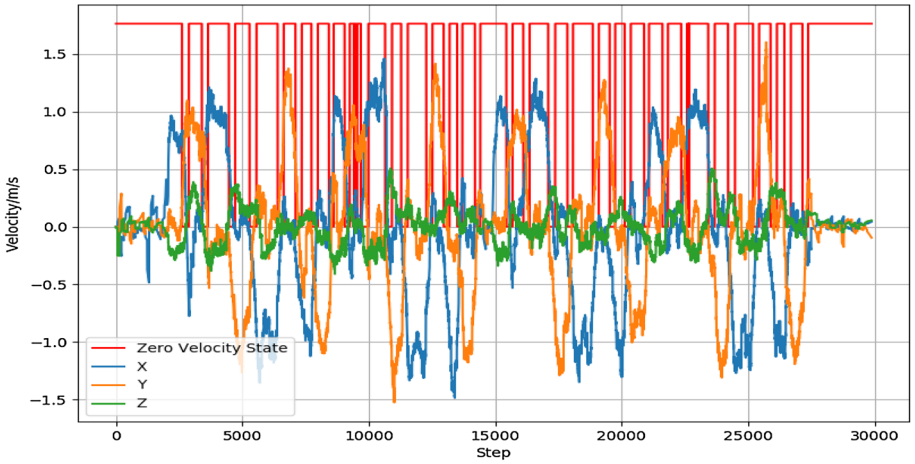

Fig. 10 The triaxial velocity not based on the pseudo-velocity constraint

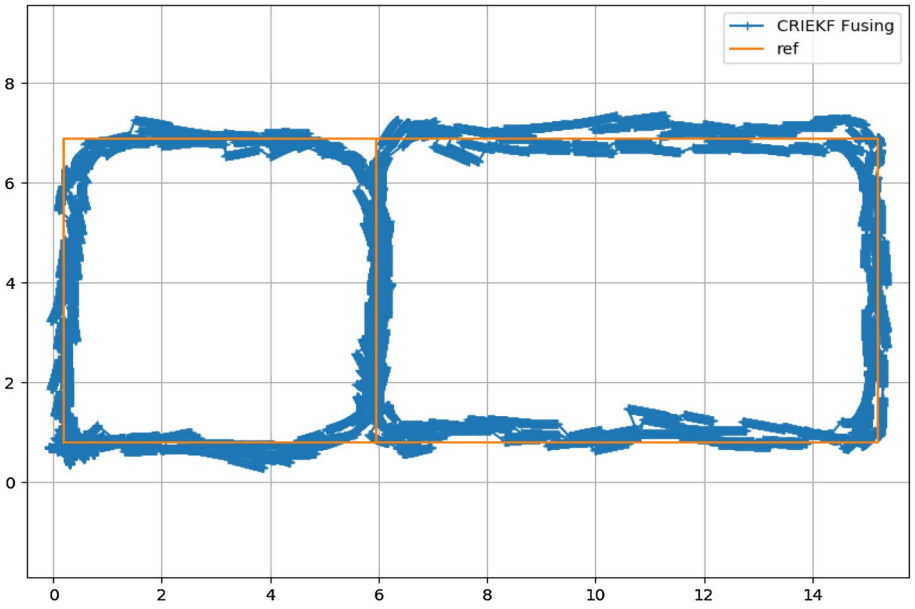

Fig. 11 The UWB/IMU fusion positioning result based on CRIEKF

s^2 and the Z axis under the plane constraint was controlled to have the same height as the UWB unit, which was around 45 cm.

3.6 Comparative analysis

As indicated in Fig. 12 and Table 1, the blue line is the UWB positioning result. However, due to the presence of numerous outliers, the mean positioning accuracy is 0.36 m. The

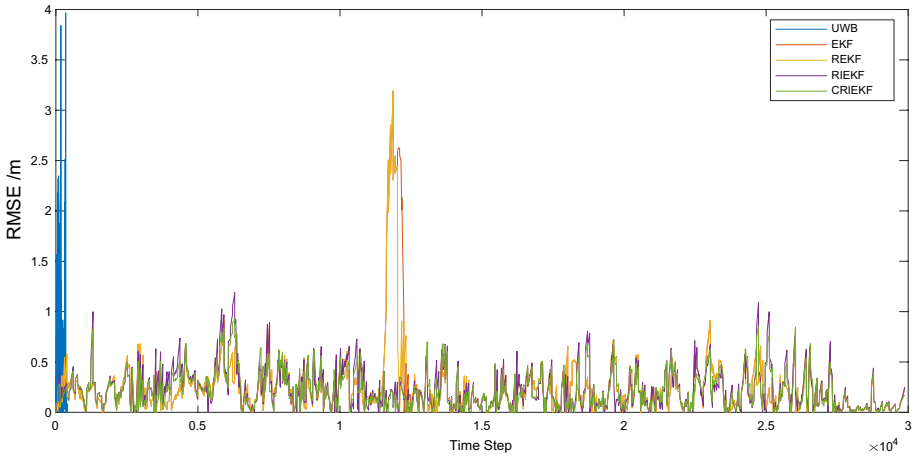

Fig. 12 The positioning result based on different solutions

Table 1 Positioning error analysis for different solutions

	UWB	EKF	REKF	RIEKF	CRIEKF
Min. error/m	0.02	0.01	0.01	0.00	0.00
Mean error/m	0.36	0.30	0.28	0.25	0.21
Max. error/m	3.98	3.18	3.19	1.18	0.92

orange line indicates the fusion positioning result based on the standard EKF algorithm with a mean positioning error of 0.30 m. The yellow line stands for the REKF-based positioning result with a mean positioning accuracy of 0.28 m. The purple line is the RIEKF-based positioning result with a mean positioning accuracy of 0.25 m, and the green line is the CRIEKF-based positioning result with a mean positioning accuracy of 0.21 m.

Figure 13 shows the cumulative probability density of each trajectory. Each color stands for the same algorithm as mentioned above. The comparison between RIEKF algorithm and CRIEKF algorithm shows that there's no big difference in the cumulative probability between these two algorithms when the error is minor. However, if it exceeds 0.9 m, cumulative probability error still arises in the RIEKF algorithm. But the maximum cumulative probability error is just 0.92 m in the CRIEKF algorithm. It reflects that the CRIEKF algorithm has better stability with a relatively smoother trajectory in the positioning process. Similar to this, the other algorithms can be ranked according to the accuracy from high to low: RIEKF, REKF, EKF, and UWB.

4 Conclusion

An IMU/UWB fusion positioning method that can achieve high positioning accuracy and stability in NLOS environments is introduced in this paper. Firstly, based on the CRIEKF algorithm proposed in this paper, both of the dynamic model and the observation model are illustrated. The experiment has proved that the CRIEKF algorithm proposed in this

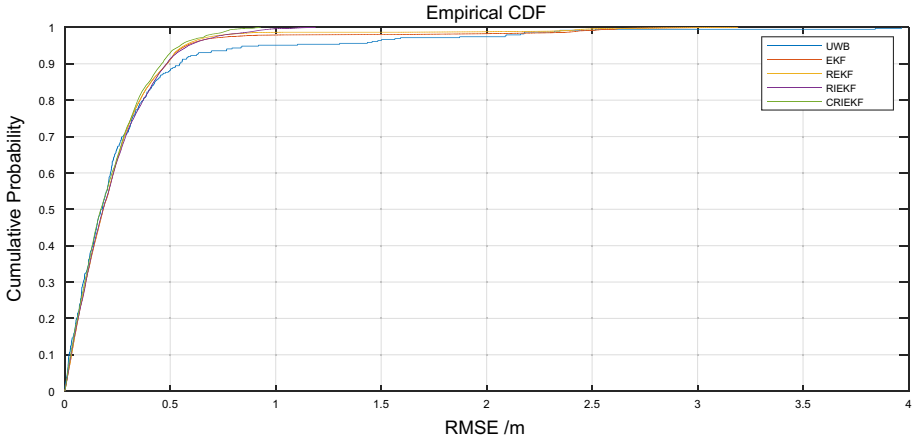

Fig. 13 The positioning CDF for different solutions

paper has the highest positioning accuracy and robustness compared with the other algorithms. As our algorithm can effectively restrain the reduction of positioning accuracy caused by non-Gaussian noise, it can be universally applied. In the future, aiming at the requirement of more complex industrial applications, the positioning algorithm based on machine learning will be explored to improve the positioning accuracy and robustness by training the latent model in the learning-based positioning problem.

Acknowledgements This work was supported by the National Natural Science Foundation of China under grant number 41674030 and China Postdoctoral Science Foundation under grant number 2016M601909 and the grand of China Scholarship Council.

References

Ascher C, Zwirello L, Zwick T, Trommer G (2011) Integrity monitoring for UWB/INS tightly coupled pedestrian indoor scenarios. In: International conference on indoor positioning and indoor navigation, pp 1–6

Benini A, Mancini A, Longhi S (2013) An IMU/UWB/vision-based extended Kalman filter for mini-UAV localization in indoor environment using 802.15.4a wireless sensor network. J Intell Robot Syst 70(1):461–476

Blanco JL, Galindo C, Ortiz-De-Galisteo A, Moreno FA (2009) Mobile robot localization based on ultra-wide-band ranging: a particle filter approach. Robot Auton Syst 57(5):496–507

Fan Q, Wu Y, Jing H, Lei W, Yu Z, Zhou L (2014) Integrated navigation fusion strategy of INS/UWB for indoor carrier attitude angle and position synchronous tracking. Sci World J 2014:215–303

Fan Q, Sun B, Sun Y, Zhuang X (2017a) Performance enhancement of mems-based ins/UWB integration for indoor navigation applications. IEEE Sens J 17(10):3116–3130

Fan Q, Sun B, Sun Y, Wu Y, Zhuang X (2017b) Data fusion for indoor mobile robot positioning based on tightly coupled ins/UWB. J Navig 70(5):1–19

Fischer C, Sukumar PT, Hazas M (2013) Tutorial: implementing a pedestrian tracker using inertial sensors. IEEE Pervasive Comput 12(2):17–27

García E, Poudereux P, Álvaro Hernández Ureña J, Gualda D (2015) A robust UWB indoor positioning system for highly complex environments. In: IEEE international conference on industrial technology. IEEE, pp 3386–3391

Hol JD, Dijkstra F, Luinge H, Schon TB (2009) Tightly coupled UWB/IMU pose estimation. In: IEEE international conference on ultra-wideband, pp 688–692

Johnson ME, Sathyan T (2011) Improved orientation estimation in complex environments using low-cost inertial sensors. In: Proceedings of the, international conference on information fusion. IEEE, pp 1–8
Li X, Wang J, Liu C (2015) A bluetooth/pdr integration algorithm for an indoor positioning system. Sensors 15(10):24862–24885
Li X, Wang J, Liu C, Zhang L, Li Z (2016) Integrated WiFi/PDR/smartphone using an adaptive system noise extended Kalman filter algorithm for indoor localization. ISPRS Int J Geo-Inf 5(2):8
Li X, Wang Y, Khoshelham K (2019) Comparative analysis of robust extended kalman filter and incremental smoothing for uwb/pdr fusion positioning in nlos environments. Acta Geodaetica Geophys 54(5):387
Nummiaro K, Koller-Meier E, Gool LV (2003) An adaptive color-based particle filter. Image Vis Comput 21(1):99–110
Santoso F, Redmond SJ (2015) Indoor location-aware medical systems for smart homecare and telehealth monitoring: state-of-the-art. Physiological Measurement 36(10):R53
Savioli A, Goldoni E, Savazzi P, Gamba P (2013) Low complexity indoor localization in wireless sensor networks by UWB and inertial data fusion. Comput Sci 52(4):723–732
Sczyslo S, Schroeder J, Galler S, Kaiser T (2008) Hybrid localization using UWB and inertial sensors. In: IEEE international conference on ultra-wideband, vol 3. IEEE Xplore, pp 89–92
Titterton DH, Weston JL (2004) Strapdown inertial navigation technology. Institution of Electrical Engineers, London
Wang Y, Li X (2017) The IMU/UWB fusion positioning algorithm based on a particle filter. ISPRS Int J Geo-Inf 6(8):235
Wang J, Gao Y, Li Z, Meng X, Hancock CM (2016) A tightly-coupled GPS/INS/UWB cooperative positioning sensors system supported by v2i communication. Sensors 16(7):E944
Wang X, Hoseinnezhad R, Gostar AK, Rathnayake T, Xu B, Bab-Hadiashar A (2018) Multi-sensor control for multi-object bayes filters. Sig Process 142:260–270
Xu Y, Chen X (2016) Range-only UWB/ins tightly integrated navigation method for indoor pedestrian. Chin J Sci Instru 37(8):142–148
Xu Y, Chen X, Cheng J, Zhao Q, Wang Y (2016) Improving tightly-coupled model for indoor pedestrian navigation using foot-mounted IMU and UWB measurements. In: Instrumentation and measurement technology conference proceedings. IEEE
Zhang J, Shen C (2016) Research on UWB indoor positioning in combination with TDOA improved algorithm and Kalman filtering. Mod Electron Tech 39(13):1–5
Zwirello L, Ascher C, Trommer GF, Zwick T (2011) Study on UWB/INS integration techniques. In: Positioning navigation and communication. IEEE Xplore, pp 13–17